Prospective-gated cardiac micro-CT imaging of free-breathing mice using carbon nanotube field emission x-ray

Guohua Cao[a] and Laurel M. Burk
Department of Physics and Astronomy, University of North Carolina, Chapel Hill, North Carolina 27599

Yueh Z. Lee
Department of Physics and Astronomy, University of North Carolina, Chapel Hill, North Carolina 27599 and Department of Radiology, University of North Carolina, Chapel Hill, North Carolina 27599

Xiomara Calderon-Colon and Shabana Sultana
Curriculum in Applied Sciences and Engineering, University of North Carolina, Chapel Hill, North Carolina 27599

Jianping Lu
Department of Physics and Astronomy, University of North Carolina, Chapel Hill, North Carolina 27599 and Curriculum in Applied Sciences and Engineering, University of North Carolina, Chapel Hill, North Carolina 27599

Otto Zhou[b]
Department of Physics and Astronomy, University of North Carolina, Chapel Hill, North Carolina 27599; Curriculum in Applied Sciences and Engineering, University of North Carolina, Chapel Hill, North Carolina 27599; and Lineberger Comprehensive Cancer Center, University of North Carolina, Chapel Hill, North Carolina 27599

(Received 21 December 2009; revised 19 August 2010; accepted for publication 2 September 2010; published 17 September 2010)

Purpose: Carbon nanotube (CNT) based field emission x-ray source technology has recently been investigated for diagnostic imaging applications because of its attractive characteristics including electronic programmability, fast switching, distributed source, and multiplexing. The purpose of this article is to demonstrate the potential of this technology for high-resolution prospective-gated cardiac micro-CT imaging.

Methods: A dynamic cone-beam micro-CT scanner was constructed using a rotating gantry, a stationary mouse bed, a flat-panel detector, and a sealed CNT based microfocus x-ray source. The compact single-beam CNT x-ray source was operated at 50 KVp and 2 mA anode current with 100 μm $\times$ 100 μm effective focal spot size. Using an intravenously administered iodinated blood-pool contrast agent, prospective cardiac and respiratory-gated micro-CT images of beating mouse hearts were obtained from ten anesthetized *free-breathing* mice in their natural position. Four-dimensional cardiac images were also obtained by gating the image acquisition to different phases in the cardiac cycle.

Results: High-resolution CT images of beating mouse hearts were obtained at 15 ms temporal resolution and 6.2 lp/mm spatial resolution at 10% of system MTF. The images were reconstructed at 76 μm isotropic voxel size. The data acquisition time for two cardiac phases was 44 ± 9 min. The CT values observed within the ventricles and the ventricle wall were 455 ± 49 and 120 ± 48 HU, respectively. The entrance dose for the acquisition of a single phase of the cardiac cycle was 0.10 Gy.

Conclusions: A high-resolution dynamic micro-CT scanner was developed from a compact CNT microfocus x-ray source and its feasibility for prospective-gated cardiac micro-CT imaging of free-breathing mice under their natural position was demonstrated. © *2010 American Association of Physicists in Medicine*. [DOI: 10.1118/1.3491806]

Key words: cardiac imaging, micro-CT, free-breathing, x-ray source, carbon nanotube

I. INTRODUCTION

Cardiac imaging plays an important role in the study of cardiovascular diseases using small-animal models. Among the different cardiac imaging modalities, micro-CT is attractive because of its high geometric accuracy, relatively fast scanning time, and cost-effectiveness.[1,2] However, obtaining CT images of a beating mouse heart at high resolution is challenging because of its small size (the left ventricle of an adult mouse is less than 4 mm in diameter) and the rapid cardiac and respiratory motions (up to 600 heartbeats per minute and ~160 breaths per minute). To reduce the motion-induced artifacts, both physiological gating and very short x-ray exposure are required.

Recent advances in micro-CT technologies have enabled *in vivo* CT imaging of the beating mouse heart using either synchrotron[3] or high-power clinical x-ray tubes.[4,5] Sera

et al.[3] reported high-resolution cardiac micro-CT images at 10 ms temporal resolution and 12 μm voxel size using monochromatic synchrotron radiation. It provides exquisite details of the mouse heart, but requires access to remote synchrotron facilities.[3] Badea *et al.*[4] used a customized micro-CT system with an angiography x-ray tube (Philips SRO 09 50) operated at 12 kW (80 kVp and 150 mA) to acquire cardiac images at 10 ms temporal resolution and 90 μm voxel size. To reduce source penumbral blurring (1 mm focal spot size), a nearly unity geometry magnification is used. Both systems require the mouse to be mechanically ventilated, positioned vertically, and rotated throughout the scan to obtain projection images. Ventilation, while allowing complete control of the animal's respiration, is often associated with airway trauma from intubation. By removing the underlying physiological drive to breath, ventilation makes it difficult to obtain true physiological parameters from a pulmonary physiology perspective. Drangova *et al.*[5] employed a commercial micro-CT scanner (Locus Ultra, GE Healthcare, London, Ontario, Canada) with a slip-ring gantry and an x-ray tube running at 4 kW (80 kV and 50 mA) to collect cardiac images of free-breathing mice at 12 ms temporal resolution and 150 μm voxel size. The spatial resolution is limited primarily by the blurring from the source penumbra and the fast gantry motion.[5–7]

In the experiments of Sera[3] and Badea,[4] images were acquired with prospective gating, while in Drangova's experiment,[5] retrospective gating was used. The retrospective gating technique can image the entire cardiac cycle in a single scan, but it unavoidably requires redundant projections/exposures[5] to minimize the missing view artifact for any phase in the cardiac cycle. In comparison, prospective gating has no redundant exposures, hence no wasted dose, which is important especially for longitudinal studies on the same mouse that requires repeated scanning.

Our goal is to develop a micro-CT scanner that is capable of prospective-gated cardiac imaging of free-breathing mice at both high spatial and high temporal resolutions. To obtain true physiological parameters with minimum perturbation, mice will be imaged under the free-breathing mode instead of intubation and will be placed in their more natural prone position without rotation. From the engineering perspective, the newly developed carbon nanotube (CNT) based field emission x ray offers an attractive approach for prospective gating. Because x-ray exposure in this case is controlled electronically rather than by either mechanical shutter or grid-control as in the case of the current thermionic sources, it can be readily gated to the natural *nonperiodic* physiological signals with microsecond resolution and minimum delay.[8] The technology further enables the fabrication of spatially distributed source arrays that can produce a scanning x-ray beam without mechanical motion, which is now being actively investigated for a variety of medical imaging devices[9–11] including stationary micro-CT scanners with ultrahigh scanning speed.[12]

We have previously reported the development of a micro-CT scanner using a single-beam CNT microfocus x-ray source housed in a large and stationary vacuum chamber.[13,14] Using this scanner with the stationary source and detector geometry, we demonstrated the feasibility of high-resolution respiratory-gated micro-CT imaging of free-breathing mice.[14] With the new development of a compact CNT microfocus x-ray source and improvement in the tube current and stability, we have designed and assembled a compact rotating-gantry based micro-CT scanner with a stationary mouse bed.[15] In this paper, we demonstrate this scanner's applicability for prospective-gated cardiac micro-CT imaging. Additionally, we show that dynamic cardiac CT images of the same anesthetized mouse can be acquired under free-breathing setting with both high temporal and high spatial resolutions.

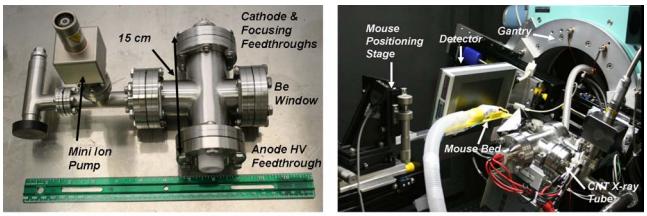

FIG. 1. Pictures of (a) the compact CNT field emission microfocus x-ray tube and (b) the desktop *in vivo* micro-CT scanner that consists of the CNT field emission microfocus x-ray tube, a flat-panel detector, a small-diameter rotating gantry, and a stationary mouse bed. The x-ray tube's body dimension is 150 mm × 70 mm × 70 mm.

II. MATERIALS AND METHODS

II.A. The desktop dynamic micro-CT scanner based on a compact CNT x-ray tube

The compact CNT x-ray tube (body dimension is 150 mm × 70 mm × 70 mm) shown in Fig. 1(a) was developed based on an experimental prototype reported in our previous publications.[14,15] It has the same electron focusing design which has been described in detail elsewhere.[16] Since the CNT electron emission is controlled by the electrical field, x rays can be easily switched on or off within microseconds[8] by applying or removing a low voltage on those CNTs, therefore allowing the x-ray exposure to be readily synchronized with an external triggering signal such as the nonperiodic respiration signal of a free-breathing mouse.[14] The current CNT x-ray tube benefits from the progress we recently made on the performance of the CNT cathodes.[17] The x-ray tube can now be operated reliably at 50 kVp and 2 mA anode current with 100 μm effective focal spot size. The anode material is tungsten and the x-ray window is 0.2 mm thick beryllium foil.

Using this compact CNT x-ray source, a desktop dynamic micro-CT scanner was built from a small-bore goniometer (Huber 430, Germany). Its relatively small size allows the entire scanner to be shielded in a desktop enclosure. The inner view of the micro-CT scanner is shown in Fig. 1(b). A commercial flat-panel detector (C7940DK-02, Hamamatsu) was used to capture x-ray images. The micro-CT scanner rotates the source-detector pair around a stationary object to collect images. During imaging, the animal was placed hori-

zontally in a custom-made mouse bed, which is attached to a homemade positioning stage. The positioning stage has three-axis linear translation to ensure that the object is positioned exactly at the isocenter and aligned with the axis of rotation. The positioning stage has a long travel distance (200 mm) in the z-axis (i.e., the axis of rotation), so that the bed can be translated completely outside the system FOV. A computer interface was developed under LABVIEW (National Instruments, Austin, TX) to automate the image acquisition process.

The scanner was optimized for high temporal resolution by reducing the source-to-detector distance (SDD) as short as possible while taking into consideration other important aspects of the system performance including the system spatial resolution, cone angle, size of FOV, and beam hardening. To reduce the beam hardening, the x-ray beam from the CNT x-ray tube was filtered by a 0.5 mm thick aluminum plate. The detector was configured to acquire projection images of dimension 1200×1200 at 50 μm $\times$ 50 μm pixel resolution and 1 Hz (500 ms integration time and 470 ms readout time). The source-to-object distance was 120 mm and the object-to-detector distance was 40 mm, resulting in a SDD of 160 mm and a geometry magnification of 1.3. This scanner geometry, along with the detector configuration, provided an effective system FOV of 46 mm $\times$ 46 mm and an effective digital sampling of 38 μm $\times$ 38 μm at the object plane. Images were reconstructed with a modified Feldkamp algorithm[18] using a commercial software package (COBRA EXXIM, Exxim Computing Corp., Livermore, CA). The performance of the micro-CT scanner was evaluated by MTF and contrast-to-noise ratio (CNR) analyses using a commercial 10 μm tungsten wire phantom (QRM, Nuremburg, Germany), a custom-made CNR phantom, and the analysis procedures described in our previous work.[14,15] The phantom studies showed that the micro-CT scanner is capable of acquiring images at a spatial resolution of 6.2 lp/mm at 10% of system MTF and an exposure time of 15 ms without compromising the CNR.

II.B. Animal preparation

Experimental procedures carried out in this study were approved by the Institutional Animal Care and Use Committee at our institution. Ten C57BL/6 mice, weighing 26.8 ± 4.1 g, were anesthetized using 1%–2% isoflurane in O_2 at a flow rate of 1.5–2 L min^{-1} from a vaporizer (Smith Medical, Waukesha, WI). The anesthetized mice were positioned prone on the custom-made mouse bed. Both the electrocardiogram (ECG) and respiratory signals, as well as the derived physiological triggers, were obtained using a physiological monitoring and triggering system (BioVet, Spin Systems, South Brisbane, Australia). The respiration signal was obtained from a respiration sensor pad placed on the surface of the animal under the abdomen to monitor the maximum respiratory movement. The ECG signal was obtained from affixing three ECG electrodes to two forepaws and one hind limb of the animal. The mice were not intubated and were allowed to breathe freely throughout the experiment.

Prior to imaging, a blood-pool contrast agent (Fenestra VC, 50 mg I/ml, Advanced Research Technologies, Inc., Montreal, Canada) was administered intravenously in a single bolus at a dose of 0.02 ml/g bodyweight as recommended by the manufacturer. This iodinated contrast agent has been shown to provide significant enhancement of the mouse vasculature (up to 700 HU at the administered dose) for up to 2 h after injection.[4,19–21] Because of this long retention time, it is possible to acquire multiple cardiac CT data sets from the same mouse after injection. To demonstrate the feasibility of prospective-gated cardiac micro-CT on free-breathing mice under the natural position, each mouse was CT scanned two times, without making any change to the animal between scans except for selecting the points in the cardiac cycle where the physiological triggers were generated using the BioVet computer interface.

II.C. Dynamic respiratory and cardiac gating

We utilized a dynamic gating method developed previously for the experimental dynamic scanner.[14] As illustrated in Fig. 2(a), the camera was running at a continuous frame rate as defined by the camera trigger signal. The x-ray exposure window signal was determined by the desired x-ray pulse width, the camera integration time, and the camera readout time. It was defined as the time window between the end of previous frame readout and the beginning of the next frame readout subtracted by the x-ray pulse width. An x-ray pulse would start within this x-ray exposure window, thus the full width of the x-ray pulse would come within the camera integration and no x rays would extend into the camera readout. In cardiac micro-CT, the x-ray pulse width, the camera integration time, and the camera readout time was 15, 500, and 470 ms, respectively. Thus the x-ray exposure window was 485 ms in duration. Although the camera integration time was much longer than the x-ray pulse width, the camera's readout noise was still 14 times smaller than the photon noise. Therefore the whole system was photon-noise limited. The x-ray pulse was fired from the CNT x-ray source if and only if there was temporal coincidence between the x-ray exposure window and the physiological trigger. An x-ray pulse would be triggered only by the leading edge of the first physiological trigger that came within the x-ray exposure window. The physiological trigger was obtained from the BioVet physiological monitoring and triggering system. If an x-ray pulse was fired, the x-ray attenuation signal was captured by the detector within the next immediate readout cycle, forming a projection image. This timing scheme has high dose efficiency because an x ray is fired on demand. It is worth pointing out that x-ray firings are based on temporal coincidence between the x-ray exposure window and the physiological triggers. The total scan time for a dynamically gated scan depends on the rate of this temporal coincidence.

In this study, the physiological trigger was generated by the simultaneous gating of both the cardiac and respiration signals. This ensures that the images were always acquired at the same phase of the cardiac cycle and within the same phase of breathing cycle. The generation of the physiological

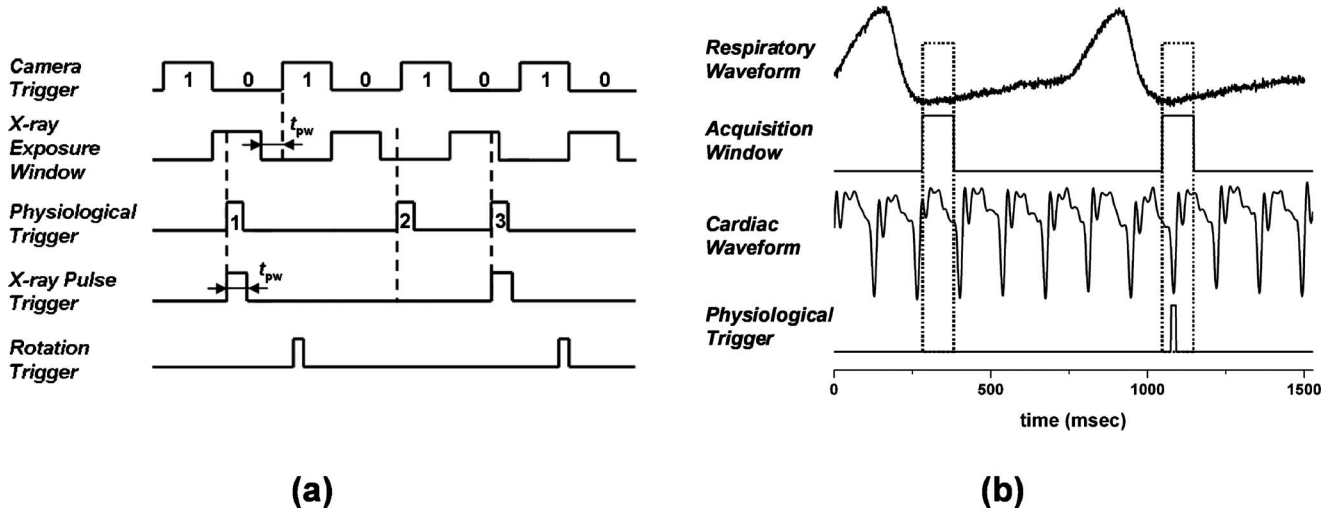

FIG. 2. (a) Illustrative timing diagram for the dynamic gating method that the micro-CT system used to gate the x-ray exposure and image acquisition to a nonperiodic physiological trigger signal. The camera readout (470 ms) and integration (500 ms) regions are designated as 1 and 0, respectively. t_{pw} is the temporal width of an x-ray pulse (15 ms for cardiac imaging). Three nonequally spaced physiological triggers (labeled as 1, 2, and 3) are used to illustrate the dynamic gating. (b) Generation of the physiological trigger corresponding to the R peak in the ECG cycle and end-expiration in the respiration cycle. The acquisition window was 100 ms in duration and defined during end-expiration of the respiration cycle. A physiological trigger was generated if an R wave occurred within the acquisition window. Physiological triggers corresponding to other points in the ECG cycle were generated by adding a constant delay after detecting the R peak. A relatively constant heart rate (±10%) was maintained throughout each scan.

trigger corresponding to the R peak in the ECG cycle and end-expiration in the breathing cycle is presented graphically in Fig. 2(b). The respiration trigger points in BioVet were set close to the baseline of the respiratory waveform, i.e., the level plateaus between breaths, so that acquisition windows of 100 ms duration were defined during end-expiration of the respiration cycle. The cardiac trigger points in BioVet were set at peaks of the R waves in the ECG. The first R wave occurring within the acquisition window generated a software trigger point in BioVet, from which the physiological trigger was derived after a user-definable delay. This user-definable delay is the time delay after the R peak and used to select the desired imaging phase in the cardiac cycle. For example, in Fig. 2(b), the targeted cardiac phase is right at the R peak, thus the user-definable delay was set to 0 ms. The physiological trigger was then subject to the temporal coincidence criterion of the dynamic gating method, as described above, to determine if an x-ray pulse should be fired and a projection image should be acquired. To demonstrate the feasibility of gating to an arbitrarily selected phase in the cardiac cycle, we performed two cardiac micro-CT scans on each mouse, one at 0 ms (user-definable delay was 0 ms) delay after the R wave (during end-diastole) and the other at 55 ms (user-definable delay was 55 ms) after the R wave (during systole). A relatively constant heart rate (±10%) was achieved by careful maintenance of the level of isoflurane anesthesia during each scan. The isoflurane percentage and the flow rate from the vaporizer were adjusted when the animal became unstable and exhibited an unsteady respiratory rate (as measured by the BioVet).

II.D. Image acquisition and reconstruction

For cardiac micro-CT, the CNT x-ray source was operated with 50 kVp anode voltage, 2 mA anode current, and 15 ms pulse width. Bright and dark images (50 for each) were collected throughout this study for detector calibration. A total of 400 projections were acquired over a circular orbit of 200° with a step angle of 0.5°. The gantry was run in the step-and-shoot mode, advancing to the next view angle only if the x-ray pulse triggering condition was satisfied and the projection image was successfully acquired. Although projection images were acquired as matrices of dimension 1200 × 1200 at an effective digital sampling of 38 μm × 38 μm at the object plane, they were reconstructed as isotropic 600 × 600 × 600 arrays with a voxel size of 76 μm (i.e., 2× downsampling). All reconstructions were done with a Feldkamp algorithm with Parker weighting.[18,22]

To estimate the radiation dose delivered during the scans, a calibrated ion chamber (6 cm^3 active volume, model 10X5–6, Radcal, Monrovia, CA) was placed near the isocenter of the scanner and irradiated during one micro-CT scan with the same scanning parameters as those in the cardiac micro-CT scans. The accumulated radiation exposure was read out by a calibrated dosimeter (Model Accu-Pro 9096, Radcal, Monrovia, CA).

III. RESULTS

In this study, the average respiration rate and average heart rate of the ten mice after anesthetization was 101 ± 14 breaths and 418 ± 42 beats per minute, respectively. The average scanning time for the projection acquisition of one volumetric data set was 22 ± 4.5 min. The entrance dose for acquiring one volumetric data set was calculated to be 0.10 Gy, based on the entrance exposure of 10.85 R that was measured at the isocenter. Therefore, the data acquisition time for two cardiac phases was 44 ± 9 min and the entrance

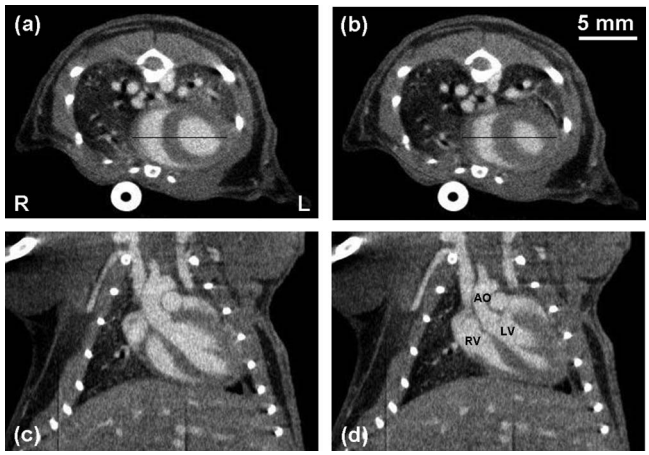

FIG. 3. [(a) and (b)] Axial and [(c) and (d)] coronal slice images of a C57BL/6 mouse at [(a) and (c)] 0 and [(b) and (d)] 55 ms after the R wave. All images have the same display window and level. The scanning parameters were 50 kVp, 2 mA, 15 ms pulse width, and 400 views over 200° at a step angle of 0.5°. These images represent 76 μm sections taken at the same slice locations from the 3D volumes reconstructed at each time point. The voxel spacing in-plane is also 76 μm. The major anatomic structures of the cardiopulmonary vascular system are readily identified in the contrast enhanced images. The AO, LV, and RV are labeled for reference.

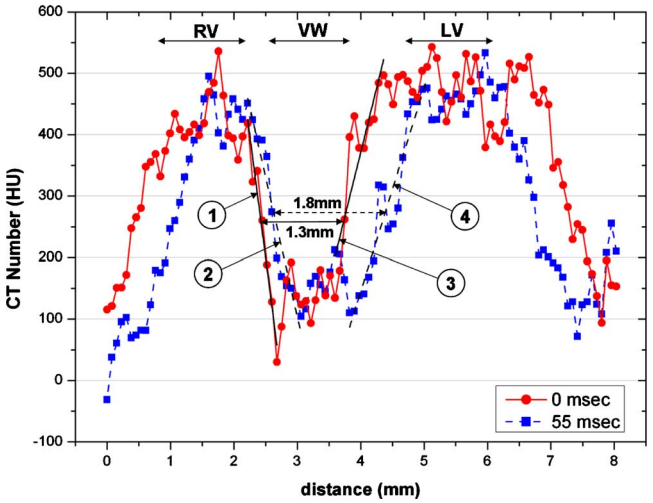

FIG. 4. Intensity profiles along the two lines within the axial images shown in Figs. 3(a) and 3(b). For each intensity profile, the two boundary regions between the ventricles and the ventricle wall were performed with a linear fit. The fitting slopes are shown in Table I. The three (RV, VW, and LV) sections of the line profiles are labeled in the plot. The width at the mid-height of the VW section changed from 1.3 mm at 0 ms to 1.8 mm at 55 ms, representing a change of 0.5 mm in the ventricle wall thickness from diastole to systole.

dose for two cardiac CT scans gated at two different points in the cardiac cycle was 0.20 Gy. All animals survived the anesthesia and imaging without difficulty.

Figure 3 shows example images acquired at 0 (diastole) and 55 ms (systole) after the R wave for one of the mice. For this mouse, its respiration and cardiac rates during the scans were 115 ± 3 breaths and 437 ± 2 beats per minute, respectively. The images presented are the 76 μm axial and coronal slices taken at the same slice locations through the mouse heart. The major cardiovascular structures are readily identified in the images, including the aorta (AO), left ventricle (LV), and right ventricle (RV). The thickening of the interventricular septum (ventricle wall or VW) between diastole and systole is easily appreciated, as well as the reduction in left ventricular volume. The right ventricular volume has also decreased; however, the rotation of the heart has slightly shifted the visualized portion of the right ventricle to a slightly different plane on the coronal images. The papillary muscles and major thoracic branches of the aorta are also readily seen. The average CT values observed within the ventricles and the ventricle wall were 455 ± 49 and 120 ± 48 HU, respectively.

Therefore, the CNR between the ventricles and the ventricle wall was determined to be 6.9. The bright circular structure at the bottom of Figs. 3(a) and 3(b) is the image of a plastic tube that links the respiratory sensor pad with the BioVet acquisition module. The dark vertical lines at the bottom of Figs. 3(c) and 3(d) were caused by a small block of detector pixels with nonlinear exposure response. It could be corrected by an improved method for flat-field correction of the x-ray detector.[23]

Figure 4 shows the intensity profiles along the two lines in Figs. 3(a) and 3(b). Those two lines cut through the ventricle wall and across both the left and right ventricles, thus the intensity profiles can be used to show the sharpness of the ventricle boundaries. The sharpness of the boundary regions between the ventricles and the ventricle wall was estimated by linear fits. A successful gating would limit the blurs induced by the cardiac motion, resulting in a sharper boundary and a steeper fitting slope. The sharpest boundary was found between the right ventricle and the ventricle wall at 0 ms, with a slope of -797 HU/mm. Overall, the slopes at 0 ms (during diastole) are steeper than those at 55 ms (during systole). This can be explained by the fact that heart contraction during systole happens faster than heart expansion during diastole.

IV. DISCUSSION AND CONCLUSION

In this paper, we reported a compact rotating gantry micro-CT scanner with a CNT based field emission microfocus x-ray source with high spatial and high temporal resolutions. We further demonstrated its capability for high-resolution prospective-gated cardiac micro-CT imaging of free-breathing mice under their natural position without forced ventilation. By gating prospectively at different points of the cardiac cycle, dynamic 3D cardiac images in free-breathing mice can be obtained. With free-breathing, the same mouse can be repeatedly imaged over time with minimum perturbation. Free-breathing allows for visualizing the mouse lungs and hearts in their natural states, thus enabling observation of the natural evolution of lung and heart diseases.[24] Overall, the imaging technique presented here is capable of high-quality cardiac imaging of a beating mouse heart, under typical physiological conditions, and without the necessity to intubate the animal or place it in an unnatural position. A similar imaging approach has been reported pre-

TABLE I. Slopes of the four boundary regions as labeled in Fig. 4. Unit is HU/mm.

Segment	Slope
1	−797
2	−454
3	418
4	331

viously in a conference abstract[25] using a commercial micro-CT scanner, but no detailed information is available.

The spatial resolution of the mouse cardiac CT images collected using the present protocol is comparable to the published results obtained by prospective gating and ventilation[4] and slightly better than the results from retrospective gating.[5] In addition to the system spatial resolution, the quality of the mouse cardiac CT images also depends on the cycle-to-cycle repeatability of the respiratory and cardiac motions, which has been shown by a recent study to be on the order of 50–100 μm.[26] Thus it is desirable for the micro-CT scanner to have a system spatial resolution in the comparable range. The 10% system MTF of the present scanner is 6.2 lp/mm, as compared to 1.9–3.1 lp/mm of the systems used for the prior cardiac micro-CT imaging studies.[5–7,27,28] The high spatial resolution is mainly attributed to the small focal spot size of the x-ray tube and the moderate geometry magnification. The image quality also depends on the object motion within a single x-ray exposure, which is directly related to the system temporal resolution. The CNT based scanner is presently operated at 15 ms temporal resolution, compared to 10–12 ms used in the prior studies.[4,5,27] In principle, a higher temporal resolution can further reduce the motion blur, leading to sharper images. This is supported by the fact that the slopes of the intensity line profiles in the diastole phase are steeper than those in the systole phase where the cardiac motion is faster (see Fig. 4 and Table I). At 15 ms temporal resolution, this scanner seems to be capable of acquiring high-resolution cardiac CT images of mice (see Fig. 3). However, further work is needed to find out the optimum temporal resolution necessary for specific cardiac research questions.

The temporal resolution is primarily limited by the flux from the x-ray source, which is determined by the emission current from the cathode and heat load of the anode material. The CNT field emission x-ray is a new and evolving technology.[16,29] Through improvement in the CNT field emission cathode[17] and the source design,[15] we have increased the flux to the current level of 100 W at 100 μm effective focal spot size with long-term stability. At this spot size, the maximum continuous x-ray tube power from the anode heat load limit perspective is 161 W according to an empirical estimation[30] and 283 W according to a theoretical estimation.[31] Therefore, the flux of the current CNT x-ray tube can potentially be increased further by 61%–183% through optimization of the CNT cathode. This will increase the temporal resolution to 9.3–5.3 ms without modifying the system design or compromising the CNR and spatial resolution, which will further enhance the image quality. At a fixed x-ray tube power, there is a trade-off between the temporal resolution and the CNR. Increasing the temporal resolution by reducing the x-ray exposure time reduces the amount of x-ray photons per exposure and, as a result, reduces the CNR.

With the current scanning protocol (a total of 400 projections), the average data acquisition time for one volumetric CT scan was 22 min. The scanning time depends on two temporal coincidence criteria: One between the QRS complex of the ECG and the acquisition window placed at a specified phase of the respiration cycle and the other between the physiological trigger and the x-ray exposure window. The latter can be increased by using a detector with faster readout. As illustrated in Fig. 2(a), a shorter detector readout time can lead to a longer x-ray exposure window for the same detector frame rate or a higher occurrence rate of the same x-ray exposure window with a faster detector frame rate. Both will result in a better chance of coincidence between the x-ray exposure window and the physiological trigger, hence shorter data acquisition time.

At the current power level (50 kVp and 2 mA), the CNT x-ray tube in this scanner has been used for more than 800 CT scans in 12 months without failure nor degradation of the flux or noticeable drifting of the focal spot size. The extraction voltage was increased by ~300 V to maintain the constant emission current. Based on its performance and our previous experiences, we estimated the operation lifetime of this CNT x-ray tube at the present power level and workload should be more than 2 yr. With improvement of the CNT cathode and the x-ray source fabrication, the lifetime of the source can be further improved.

In conclusion, using a CNT field emission microfocus x-ray tube, we have developed a compact rotating gantry micro-CT scanner that allows for high-resolution cardiac micro-CT imaging of mice. This high-quality imaging was achieved with mice under free-breathing setting, in their natural position, stationary, and with prospective gating. The current compact design with a single-beam CNT x-ray source offers ease of electronic control and delivers a better spatial resolution than the reported values in the published cardiac micro-CT studies using the state-of-the-art commercial rotating gantry micro-CT scanner with slip-ring design and high-power x-ray source.[5] As a new technology in its embryonic stage, the performance of the CNT based micro-CT scanner can be further improved in several fronts. With a higher emission current from the CNT cathode, the system temporal resolution can be increased to be better than 10 ms while maintaining the CNR used in the present study. The development of the spatially distributed CNT x-ray source array technology can potentially lead to a stationary micro-CT scanner with a much faster scanning speed[12] and with multiple energy capability.

ACKNOWLEDGMENTS

The authors would like to thank Dr. E. Kang and Dr. M. Willis of the McCallister Heart Institute at UNC for provid-

ing the wild-type mouse samples and Dr. J. Zhang and Dr. S. Chang of the Department of Radiation Oncology at UNC for helping on the dose measurement. The authors would also like to thank Dr. D.S. Lalush of the Department of Biomedical Engineering at NCSU, Dr. E.A. Hoffman of the Department of Radiology at University of Iowa, Dr. W. Lin, Dr. Y. Hong, and Dr. B. Yoder of the Department of Biomedical Engineering at UNC for their helpful discussions, and Dr. H. Geng and Dr. B. Gao of Xintek for assistance in carbon nanotube cathode fabrication. The authors acknowledge support from NIH-NIBIB (Grant No. 4R33EB004204-01), NIH-NCI (Grant No. U54CA119343), and Xintek, Inc.

[a]Electronic mail: gcao@physics.unc.edu
[b]Electronic mail: zhou@physics.unc.edu

[1]C. T. Badea, E. Bucholz, L. W. Hedlund, H. A. Rockman, and G. A. Johnson, "Imaging methods for morphological and functional phenotyping of the rodent heart," Toxicol. Pathol. **34**, 111–117 (2006).
[2]K. Johnson, "Introduction to rodent cardiac imaging," ILAR J. **49**, 27–34 (2008).
[3]T. Sera, H. Yokota, K. Fujisaki, K. Fukasaku, H. Tachibana, K. Uesugi, N. Yagi, and R. Himeno, "Development of high-resolution 4D in vivo-CT for visualization of cardiac and respiratory deformations of small animals," Phys. Med. Biol. **53**, 4285–4301 (2008).
[4]C. T. Badea, B. Fubara, L. W. Hedlund, and G. A. Johnson, "4-D micro-CT of the mouse heart," Mol. Imaging **4**, 110–116 (2005).
[5]M. Drangova, N. L. Ford, S. A. Detombe, A. R. Wheatley, and D. W. Holdsworth, "Fast retrospectively gated quantitative four-dimensional (4D) cardiac micro computed tomography imaging of free-breathing mice," Invest. Radiol. **42**, 85–94 (2007).
[6]L. Y. Du, J. Umoh, H. N. Nikolov, S. I. Pollmann, T.-Y. Lee, and D. W. Holdsworth, "A quality assurance phantom for the performance evaluation of volumetric micro-CT systems," Phys. Med. Biol. **52**, 7087–7108 (2007).
[7]W. Ross, D. D. Cody, and J. D. Hazle, "Design and performance characteristics of a digital flat-panel computed tomography system," Med. Phys. **33**, 1888–1901 (2006).
[8]Y. Cheng, J. Zhang, Y. Z. Lee, B. Gao, S. Dike, W. Lin, J. Lu, and O. Zhou, "Dynamic radiography using a carbon-nanotube-based field-emission x-ray source," Rev. Sci. Instrum. **75**, 3264–3267 (2004).
[9]G. Yang, R. Rajaram, G. Cao, S. Sultana, Z. Liu, D. Lalush, J. Lu, and O. Zhou, in Medical Imaging 2008: Proceedings of the Physics of Medical Imaging Conference, 2008, edited by J. Hsieh and E. Samei, Vol. 6913, p. 69131A.
[10]X. Qian, R. Rajaram, X. Calderon-Colon, G. Yang, T. Phan, D. S. Lalush, J. Lu, and O. Zhou, "Design and characterization of a spatially distributed multibeam field emission x-ray source for stationary digital breast tomosynthesis," Med. Phys. **36**, 4389–4399 (2009).
[11]J. S. Maltz, F. Sprenger, J. Fuerst, A. Paidi, F. Fadler, and A. R. Bani-Hashemi, "Fixed gantry tomosynthesis system for radiation therapy image guidance based on a multiple source x-ray tube with carbon nanotube cathodes," Med. Phys. **36**, 1624–1636 (2009).
[12]R. Peng, J. Zhang, X. Calderon-Colon, S. Wang, S. Sultana, S. Chang, J. P. Lu, and O. Zhou, in Medical Imaging 2009: Proceedings of the Physics of Medical Imaging Conference, 2009, edited by E. Samei and J. Hsieh, Vol. 7258, pp. 725847.
[13]G. Cao, Y. Z. Lee, Z. Liu, R. Rajaram, R. Peng, X. Calderon-Colon, L. An, P. Wang, T. Phan, D. Lalush, J. Lu, and O. Zhou, in Medical Imaging 2008: Proceedings of the Physics of Medical Imaging Conference, 2008, edited by J. Hsieh and E. Samei, Vol. 6913, p. 691304.
[14]G. Cao, Y. Z. Lee, R. Peng, Z. Liu, R. Rajaram, X. Calderon-Colon, L. An, P. Wang, T. Phan, S. Sultana, D. S. Lalush, J. P. Lu, and O. Zhou, "A dynamic micro-CT scanner based on a carbon nanotube field emission x-ray source," Phys. Med. Biol. **54**, 2323–2340 (2009).
[15]G. Cao, X. Calderon-Colon, P. Wang, L. Burk, Y. Z. Lee, R. Rajaram, S. Sultana, D. Lalush, J. Lu, and O. Zhou, in Medical Imaging 2009: Proceedings of the Physics of Medical Imaging Conference, 2009, edited by E. Samei and J. Hsieh, Vol. 7258, p. 72585Q.
[16]Z. Liu, G. Yang, Y. Lee, D. Bordelon, J. Lu, and O. Zhou, "Carbon nanotube based microfocus field emission x-ray source for microcomputed tomography," Appl. Phys. Lett. **89**, 103111 (2006).
[17]X. Calderón-Colón, H. Geng, B. Gao, L. An, G. Cao, and O. Zhou, "A carbon nanotube field emission cathode with high current density and long-term stability," Nanotechnology **20**, 325705 (2009).
[18]L. A. Feldkamp, L. C. Davis, and J. W. Kress, "Practical cone-beam algorithm," J. Opt. Soc. Am. A **1**, 612–619 (1984).
[19]D. Bakan, J. Weichert, M. Longino, and R. Counsell, "Polyiodinated triglyceride lipid emulsions for use as hepatoselective contrast agents in CT—Effects of physicochemical properties on biodistribution and imaging profiles," Invest. Radiol. **35**, 158–169 (2000).
[20]D. Bakan, F. Lee, J. Weichert, M. Longino, and R. Counsell, "Hepatobiliary imaging using a novel hepatocyte-selective CT contrast agent," Acad. Radiol. **9**, S194–S199 (2002).
[21]N. Ford, K. Graham, A. Groom, I. MacDonald, A. Chambers, and D. Holdsworth, "Time-course characterization of the computed tomography contrast enhancement of an iodinated blood-pool contrast agent in mice using a volumetric flat-panel equipped computed tomography scanner," Invest. Radiol. **41**, 384–390 (2006).
[22]D. L. Parker, "Optimal short scan convolution reconstruction for fan beam CT," Med. Phys. **9**, 254–257 (1982).
[23]A. L. C. Kwan, J. A. Seibert, and J. M. Boone, "An improved method for flat-field correction of flat panel x-ray detector," Med. Phys. **33**, 391–393 (2006).
[24]N. L. Ford, H. N. Nikolov, C. J. D. Norley, M. M. Thornton, P. J. Foster, M. Drangova, and D. W. Holdsworth, "Prospective respiratory-gated micro-CT of free breathing rodents," Med. Phys. **32**, 2888–2898 (2005).
[25]T. C. Doyle, A. Y. Sheikh, M. K. Sheikh, F. Cao, P. C. Yang, R. C. Robbins, and J. C. Wu, "Longitudinal assessment of murine cardiac function using in vivo contrast-enhanced gated microCT," presented at the Proceedings of the Joint Molecular Imaging Conference 2007, Providence, Rhode Island, 2007.
[26]W. Maï, C. T. Badea, C. T. Wheeler, L. W. Hedlund, and G. A. Johnson, "Effects of breathing and cardiac motion on spatial resolution in the microscopic imaging of rodents," Magn. Reson. Med. **53**, 858–865 (2005).
[27]C. Badea, L. W. Hedlund, and G. A. Johnson, "Micro-CT with respiratory and cardiac gating," Med. Phys. **31**, 3324–3329 (2004).
[28]S. M. Johnston, G. A. Johnson, and C. T. Badea, "Geometric calibration for a dual tube/detector micro-CT system," Med. Phys. **35**, 1820–1829 (2008).
[29]J. Zhang, Y. Cheng, Y. Z. Lee, B. Gao, Q. Qiu, W. L. Lin, D. Lalush, J. Lu, and O. Zhou, "A nanotube-based field emission x-ray source for microcomputed tomography," Rev. Sci. Instrum. **76**, 094301 (2005).
[30]M. Flynn, S. Hames, D. Reimann, and S. Wilderman, "Microfocus x-ray sources for 3D microtomography," Nucl. Instrum. Methods Phys. Res. A **353**, 312–315 (1994).
[31]D. E. Grider, A. Wright, and P. K. Ausburn, "Electron beam melting in microfocus x-ray tubes," J. Phys. D **19**, 2281–2292 (1986).